International Journal of Aeronautical and Space Sciences
https://doi.org/10.1007/s42405-019-00201-5

IJASS International Journal of Aeronautical and Space Sciences

ORIGINAL PAPER

Robust IFNTSM–ESO Control Design for Aircraft Subject to Parameter Uncertainties

Jing Zhang[1] · Jianing Yan[1,2] · Lingyu Yang[1] · Yuhan Mou[1]

Received: 29 January 2019 / Revised: 21 June 2019 / Accepted: 27 July 2019

Abstract
A comprehensive strategy that combines improved fast nonsingular terminal sliding mode (IFNTSM) control and an extended state observer (ESO) is developed to solve the problems of uncertainty in the aeronautical field. First, the IFNTSM control method is proposed to solve the singularity problem and guarantee a faster finite-time convergence speed. Second, an ESO is introduced to estimate the parameter uncertainties, and then a control scheme that combines IFNTSM and ESO is developed to overcome the drawback of large switching gains in a sliding mode controller and alleviate the chattering problem. The stability of the composite system is analyzed via the Lyapunov stability theorem. Finally, the simulation demonstrates that the composite controller accelerates the convergence speed and offers excellent robustness for complex parameter uncertainties.

Keywords Sliding mode control · Attitude control · Parameter uncertainty · Extended state observer

1 Introduction

High-precision attitude control of an aircraft is crucial for the success of a flight mission. Consequently, complex and unknown parameter uncertainties during flights make the accurate control of aircraft a challenge. Aircraft fuel consumption, fuel transfer, wing icing, and abrupt structural damage cause complex changes in the aerodynamic center of gravity (CG) and inertial parameters. These parameter uncertainties not only have an adverse impact on control performance but also can cause aircraft to lose control, which affects safety. Thus, an advanced control approach to handling parameter uncertainties is critical.

Many research institutions have undertaken research on the advanced control problem of aircraft subject to parameter uncertainties in depth. Control methods for solving the problem of uncertainty include robust control [1–4], adaptive control [5–9], optimal control [10–12], and sliding mode control [13–17]. Sliding mode control (SMC) is effective in flight control systems due to its intrinsic robustness against parameter uncertainties, effectiveness and simplicity. Bluman et al. [13] developed classical SMC strategies for a model bumblebee that hovers in the pitch plane. The results demonstrated the effectiveness of the controller in precise control while subjecting the bumblebee to non-equilibrium control inputs, uncertainties, wind gusts and wing damage. Xiong et al. [17] designed a flight control system for an unmanned aerial vehicle using a second-order SMC method. This controller tracks control for position and attitude of a vehicle under uncertainties of mass and inertia. The classical sliding modes that were previously mentioned typically select switching manifolds as asymptotical stable linear switching hyperplanes, which can guarantee only asymptotic error convergence. However, asymptotical stability may cause a slow convergence rate for high-precision control unless a strong control surface is imposed. Nonlinear switching manifolds, such as the terminal sliding mode (TSM), are developed; they can significantly improve the transient performance and enable the system

✉ Jing Zhang
zhangjing2013@buaa.edu.cn

Jianing Yan
yanjianing@buaa.edu.cn

Lingyu Yang
yanglingyu@buaa.edu.cn

Yuhan Mou
mouyh@buaa.edu.cn

[1] School of Automation Science and Electrical Engineering, Beihang University, E602, New Main Building, Xueyuan Road No. 37, Haidian District, Beijing 100191, People's Republic of China

[2] Beijing Electrical and Mechanical Engineering Design Department, Beihang University, Haidian District, Beijing 100191, People's Republic of China

Published online: 08 August 2019

states to attain the equilibrium point within a finite time [18, 19]. The TSM with nonlinear switching hyperplanes has a potential drawback. Singularity appears in some regions of the state space of the TSM methods, which prohibits practical applications. To address this problem, nonsingular terminal sliding mode control (NTSM) is developed to effectively solve the problem of singularity by transferring the trajectory to the designated area where TSM is not singular in the state space [20–22]. Feng Y. and Man Z. et al. solved the problem of singularity associated with conventional TSM by proposing a new TSM manifold for the second-order system and demonstrated that the convergence time is finite for any initial state [20].

For the conventional NTSM control method, people usually choose a sufficiently large switching gain of the NTSM to address the system uncertainties and disturbances. When the switching gains are sufficiently large, robust stabilization is theoretically achieved. Nevertheless, unmodeled dynamics and disturbances always exist in flight control systems. Therefore, large switching gains may cause chattering in real systems, which indicates that the state oscillates around the sliding manifold.

To relax the requirement on the upper bound of uncertainties, a novel comprehensive strategy that combines the improved fast nonsingular terminal sliding mode (IFNTSM) control method and extended state observer (ESO) strategies, i.e., IFNTSM–ESO, is proposed in this paper. This method offers chattering-free robust control with improved finite-time convergence. In the comprehensive IFNTSM–ESO method, an IFNTSM control method for solving the problem of singularity and guaranteeing a faster finite-time convergence speed for any initial state is developed. An ESO is introduced to overcome the drawback of large switching gains in NTSM and alleviate the chattering problem. Han first proposed the ESO [23] which has been considered in different control methods [24–27]. The stability of the method is theoretically demonstrated via the Lyapunov theorem.

The structure of the paper is organized as follows: the mathematical modeling and problem formulation are described in Sect. 2. The design and stability analysis of IFNTSM–ESO are developed in Sect. 3. In Sect. 4, simulation studies are conducted to prove the effectiveness and superiority of the IFNTSM–ESO scheme. The conclusions are discussed in Sect. 5.

2 Problem Formulation

Considering angular and linear velocity as state variables, the aircraft model [28] in body-fixed frame can be obtained as (1), which includes CG variations:

$$\begin{bmatrix} \frac{d\boldsymbol{V}_b}{dt} \\ \frac{d\boldsymbol{\omega}_b}{dt} \end{bmatrix} = \begin{bmatrix} m\mathbf{I_{3\times 3}} & -m\mathbf{D} \\ m\mathbf{D} & \mathbf{I} \end{bmatrix}^{-1} \left\{ \begin{bmatrix} \boldsymbol{F}_b \\ \boldsymbol{M}_b \end{bmatrix} - \begin{bmatrix} m\boldsymbol{\Omega} & -m\boldsymbol{\Omega}\mathbf{D} \\ m\boldsymbol{\Omega}\mathbf{D} & \boldsymbol{\Omega}\mathbf{I} - m\mathbf{V}\mathbf{D} \end{bmatrix} \begin{bmatrix} \boldsymbol{V}_b \\ \boldsymbol{\omega}_b \end{bmatrix} \right\}, \tag{1}$$

where

$$\boldsymbol{\Omega} = \begin{bmatrix} 0 & -r & q \\ r & 0 & -p \\ -q & p & 0 \end{bmatrix}, \mathbf{V} = \begin{bmatrix} 0 & -w & v \\ w & 0 & -u \\ -v & u & 0 \end{bmatrix},$$

$$\mathbf{D} = \begin{bmatrix} 0 & -\Delta z_{cg} & \Delta y_{cg} \\ \Delta z_{cg} & 0 & -\Delta x_{cg} \\ -\Delta y_{cg} & \Delta x_{cg} & 0 \end{bmatrix}, \mathbf{I} = \begin{bmatrix} I_x & -I_{xy} & -I_{xz} \\ -I_{xy} & I_y & -I_{yz} \\ -I_{xz} & -I_{yz} & I_z \end{bmatrix},$$

m represents the mass. $\mathbf{I_{3\times 3}}$ represents the 3×3 unit matrix. $\boldsymbol{\omega}_b = [p, q, r]^{\mathrm{T}}$ represents the aircraft angular velocities, and $\boldsymbol{V}_b = [u, v, w]^{\mathrm{T}}$ represents the linear velocities. $\boldsymbol{F}_b$ and $\boldsymbol{M}_b$ represent the resultant external forces and moments defined in the body-fixed coordinate system. Δx_{cg},Δy_{cg} and Δz_{cg} are the CG variations on the body axes. Matrix $\mathbf{I}$ represents the inertia tensor of aircraft.

Denoting the resultant external moment $\boldsymbol{M}_b$ as $\boldsymbol{U}$, and note that $(\boldsymbol{\Omega}\mathbf{D})^T \boldsymbol{V}_b = \boldsymbol{\Omega}\mathbf{D}\boldsymbol{V}_b - \mathbf{V}\mathbf{D}\boldsymbol{\omega}_b$, we can express the angular motion equation as (2).

$$\dot{\boldsymbol{\omega}}_b = -\mathbf{I}^{-1}\boldsymbol{\Omega}\mathbf{I}\boldsymbol{\omega}_b + \mathbf{I}^{-1}\boldsymbol{U} - \mathbf{I}^{-1}(m\boldsymbol{\Omega}\mathbf{D})^T \boldsymbol{V}_b - \mathbf{I}^{-1}m\mathbf{D}\dot{\boldsymbol{V}}_b. \tag{2}$$

Based on (2), the aerodynamic and inertial parameter uncertainties can be defined as follows:

$$\Delta\mathbf{I} = k_I\mathbf{I},$$

$$\Delta\boldsymbol{C} = \left[\Delta C_x, \Delta C_y, \Delta C_z\right]^T = k_{\boldsymbol{C}}\boldsymbol{C}_M, \tag{3}$$

where $\Delta\mathbf{I}$,$\Delta\boldsymbol{C}$ represent the inertial and aerodynamic parameter uncertainties. $\boldsymbol{C}_M$ is the aerodynamic moment coefficient of aircraft. $k_I, k_{\boldsymbol{C}}$ indicate the percentage values of the uncertainties, respectively. ΔC_x, ΔC_y, ΔC_z indicate the aerodynamic coefficient uncertainties of the roll, pitch and yaw moments, respectively.

The impact of the aerodynamic parameter uncertainties on (2) can be expressed as (4).

$$\Delta\boldsymbol{U} = QS\left[\Delta C_x b, \Delta C_y c_A, \Delta C_z b\right]^T, \tag{4}$$

where Q, S, b and c_A represent the dynamic pressure, wing area, wing span and mean aerodynamic chord, respectively.Then the angular motion equation with parameter uncertainties can be written as

$$\dot{\boldsymbol{\omega}}_b = -\mathbf{I}^{-1}\Omega\mathbf{I}\boldsymbol{\omega}_b + \mathbf{I}^{-1}\boldsymbol{U} + \mathbf{I}^{-1}\left[\Delta\boldsymbol{U} - \frac{k_I}{1+k_I}(\boldsymbol{U} + \Delta\boldsymbol{U}) - \frac{1}{1+k_I}(m\boldsymbol{\Omega}\mathbf{D})^T\boldsymbol{V}_b - \frac{1}{1+k_I}m\mathbf{D}\dot{\boldsymbol{V}}_b\right]. \tag{5}$$

The roll angle ϕ, pitch angle θ and yaw angle ψ can be written in vector form as the Euler angle $\boldsymbol{X}$. Thus, the angular velocity $\boldsymbol{\omega}_b$ satisfy the following equation:

$$\boldsymbol{\omega}_b = \mathbf{P}_{\mathbf{X}}\dot{\boldsymbol{X}}, \tag{6}$$

where

$$\mathbf{P}_{\mathbf{X}} = \begin{bmatrix} 1 & 0 & -\sin\theta \\ 0 & \cos\phi & \cos\theta\sin\phi \\ 0 & -\sin\phi & \cos\theta\cos\phi \end{bmatrix} \boldsymbol{X} = \begin{bmatrix} \phi \\ \theta \\ \psi \end{bmatrix}.$$

Differentiating the angular velocity, we have

$$\dot{\boldsymbol{\omega}}_b = \dot{\mathbf{P}}_{\mathbf{X}}\dot{\boldsymbol{X}} + \mathbf{P}_{\mathbf{X}}\ddot{\boldsymbol{X}}.$$

As $\det(\mathbf{I}) = \left(I_x I_z - I_{xz}^2\right) I_y \neq 0$, the inertia matrix $\mathbf{I}$ is invertible. When the Euler angle θ is in the definitional domain, i.e., $|\theta| < 90°$, $\det(\mathbf{P}_{\mathbf{X}}) = \cos\theta \neq 0$ always holds, then the matrix $\mathbf{P}_{\mathbf{X}}$ is invertible. Considering this analysis, as the matrixes $\mathbf{I}$ and $\mathbf{P}_{\mathbf{X}}$ are invertible, then $(\mathbf{IP}_{\mathbf{X}})^{-1}$ is existent. Thus, a new form of (5) can be obtained as (7).

$$\begin{aligned} \ddot{\boldsymbol{X}} = & -(\mathbf{IP}_{\mathbf{X}})^{-1}(\boldsymbol{\Omega}\mathbf{IP}_{\mathbf{X}} + \mathbf{I}\dot{\mathbf{P}}_{\mathbf{X}})\dot{\boldsymbol{X}} + (\mathbf{IP}_{\mathbf{X}})^{-1}\boldsymbol{U} \\ & + (\mathbf{IP}_{\mathbf{X}})^{-1}\Bigg[\Delta\boldsymbol{U} - \frac{k_I}{1+k_I}(\boldsymbol{U} + \Delta\boldsymbol{U}) \\ & - \frac{1}{1+k_I}(m\boldsymbol{\Omega}\mathbf{D})^T\boldsymbol{V}_b - \frac{1}{1+k_I}m\mathbf{D}\dot{\boldsymbol{V}}_b\Bigg]. \end{aligned} \tag{7}$$

Therefore, we can obtain the attitude equations as (8).

$$\ddot{\boldsymbol{X}} = \mathbf{F}\dot{\boldsymbol{X}} + \mathbf{B}\boldsymbol{U} + \boldsymbol{d}(t), \tag{8}$$

where

$$\mathbf{F} = -(\mathbf{IP}_{\mathbf{X}})^{-1}(\boldsymbol{\Omega}\mathbf{IP}_{\mathbf{X}} + \mathbf{I}\dot{\mathbf{P}}_{\mathbf{X}}),$$

$$\mathbf{B} = (\mathbf{IP}_{\mathbf{X}})^{-1},$$

$$\begin{aligned} \boldsymbol{d}(t) = & (\mathbf{IP}_{\mathbf{X}})^{-1}\Bigg[\Delta\boldsymbol{U} - \frac{k_I}{1+k_I}(\boldsymbol{U} + \Delta\boldsymbol{U}) \\ & - \frac{1}{1+k_I}(m\boldsymbol{\Omega}\mathbf{D})^T\boldsymbol{V}_b - \frac{1}{1+k_I}m\mathbf{D}\dot{\boldsymbol{V}}_b\Bigg], \end{aligned}$$

where $\boldsymbol{d}(t)$ represents the parameter uncertainties, which include the aerodynamic, CG and inertial impact.

3 Robust IFNTSM–ESO Control Design

To address system uncertainties, a comprehensive design of IFNTSM control and ESO is developed for aircraft with parameter uncertainties. Compared with the NTSM method, IFNTSM guarantees that equilibrium will be attained, and the convergence time of IFNTSM will be finitely improved. The system uncertainties will be effectively addressed using the IFNTSM method. An ESO is introduced to eliminate the effects of strong uncertainties and overcome the drawback of large switching gains in the NTSM. Finally, the stability of IFNTSM–ESO control methods is analyzed via the Lyapunov theorem.

3.1 IFNTSM Controller

Define $\boldsymbol{X} = \boldsymbol{x}_1$ and $\dot{\boldsymbol{X}} = \boldsymbol{x}_2$. The aircraft model (8) is rewritten as (9).

$$\begin{cases} \dot{\boldsymbol{x}}_1 = \boldsymbol{x}_2 \\ \dot{\boldsymbol{x}}_2 = \mathbf{F}\boldsymbol{x}_2 + \mathbf{B}\boldsymbol{U} + \boldsymbol{d}(t) \end{cases}, \tag{9}$$

In Eq. (9), $\boldsymbol{U}$ is the virtual control input of the aircraft, and the deflections of control surfaces can be obtained through the control allocation approach, which can allocate the desired control moments to each control surface.

The system tracking error can be written as (10).

$$\boldsymbol{e} = \boldsymbol{x}_1 - \boldsymbol{r}, \tag{10}$$

where $\boldsymbol{r}$ is the desired reference signal, which is assumed to be twice differentiable.

The NTSM concept, which is proposed in [20], can be introduced as (11).

$$\boldsymbol{s} = \boldsymbol{e} + \frac{1}{\beta}\dot{\boldsymbol{e}}^{h/g}, \tag{11}$$

where $\beta > 0$ is a design constant and g, $h(h>g)$ are positive odd integers.

Define the finite time T_{Ni} as

$$T_{Ni} = \int_0^{e_i(0)} \frac{1}{(\beta e_i)^{g/h}} de_i = \frac{|e_i(0)|^{1-g/h}}{\beta^{g/h}(1-g/h)},$$

where $e_i (i = 1,2,3)$ represents the element of the tracking error $\boldsymbol{e}$. For any initial state $e_i(0) \neq 0$, e_i will tend to be zero in the finite time T_{Ni}.

The nonlinear part of the NTSM model can deteriorate the convergence speed at some distance from equilibrium [29]. If the state variables of the system are not in the equilibrium neighborhood, the model will not prevail over the linear counterpart (setting $h = g$). An effective approach to solve the problem is to develop the IFNTSM model as (12).

$$\boldsymbol{s} = \boldsymbol{e} + \gamma\boldsymbol{e}^{mh/ng} + \alpha\boldsymbol{e}^{h/g} + \frac{1}{\beta}\dot{\boldsymbol{e}}^{h/g}, \tag{12}$$

where m, n are positive odds. The conditions $\alpha, \beta, \gamma > 0$ and $m>n$ are satisfied.

When the system state enters the sliding mode phase $\boldsymbol{s} = 0$, we obtain the following expression:

$$\dot{\boldsymbol{e}}^{h/g} = -\beta\gamma \boldsymbol{e}^{mh/ng} - \beta\alpha \boldsymbol{e}^{h/g} - \beta \boldsymbol{e}. \tag{13}$$

When state variables of a system are in the equilibrium neighborhood, i.e.,$|e_i| < 1$, IFNTSM has a fast convergence rate. The introduction of the nonlinearity term $\boldsymbol{e}^{mh/ng}$ accelerates the convergence speed when the state of the system is far from equilibrium ($|e_i| > 1$).

The convergence time of the proposed method is determined as follows:

$$T_{IFNi} = \int_0^{e_i(0)} \frac{1}{(\beta e_i + \alpha\beta e_i^{h/g} + \beta\gamma e_i^{mh/ng})^{g/h}} de_i.$$

We have $T_{IFNi} < T_{Ni}$ based on the previous equation, which indicates that the method will accelerate the convergence process. This process also guarantees that the time that is used to reach equilibrium is bounded and finite [30].

Differentiate the variable $\boldsymbol{s}$ in (12) and define the reaching law (14).

$$\dot{\boldsymbol{s}} = -\frac{h}{\beta g}\mathbf{Q_1}\boldsymbol{\varepsilon}\mathrm{sgn}(\boldsymbol{s}) \tag{14}$$

where $\mathbf{Q_1} = diag\left(\dot{e}_i^{h/g-1}\right)$ and $\boldsymbol{\varepsilon} = diag(\varepsilon_i)$, with i= 1,2,3.

Thus, we can obtain the control law (15).

$$\begin{aligned}\boldsymbol{U} = -\mathbf{B}^{-1}\Bigg[&\mathbf{F}\boldsymbol{x}_2 - \ddot{\boldsymbol{r}} + \frac{\beta g}{h}\dot{\boldsymbol{e}}^{2-h/g} + \frac{\beta\gamma m}{n}\mathbf{Q_3}\dot{\boldsymbol{e}}^{2-h/g} \\ &+ \alpha\beta\mathbf{Q_2}\dot{\boldsymbol{e}}^{2-h/g} + \boldsymbol{\varepsilon}\mathrm{sgn}(\boldsymbol{s})\Bigg],\end{aligned} \tag{15}$$

where $\mathbf{Q}_2 = diag\left(e_i^{h/g-1}\right)$ and $\mathbf{Q}_3 = diag\left(e_i^{mh/ng-1}\right)$, with i= 1,2,3.

Theorem 1 *Consider the nonlinear system described by* (9)*, with the IFNTSM control law* (15)*. The system tracking error* $\boldsymbol{e}$ *will converge to zero in a finite time if the conditions* $\varepsilon_i > |d_i(t)|$ *(*i*= 1,2,3) and* $2 > h > g > 1$, $m > n$ *are satisfied.*

Proof Select the Lyapunov function as follows:

$$V = \frac{1}{2}\boldsymbol{s}^T\boldsymbol{s}.$$

Take the derivative of V,

$$\dot{V} = \boldsymbol{s}^T\left(\dot{\boldsymbol{e}} + \frac{\gamma mh}{ng}\mathbf{Q_3}\dot{\boldsymbol{e}} + \frac{\alpha h}{g}\mathbf{Q_2}\dot{\boldsymbol{e}} + \frac{h}{\beta g}\mathbf{Q_1}\ddot{\boldsymbol{e}}\right).$$

Substitute (10) and (15) into this equation and obtain the following equation:

$$\begin{aligned}\dot{V} &= \boldsymbol{s}^T\Big\{\dot{\boldsymbol{e}} + \frac{\gamma mh}{ng}\mathbf{Q_3}\dot{\boldsymbol{e}} + \frac{\alpha h}{g}\mathbf{Q_2}\dot{\boldsymbol{e}} + \frac{h}{\beta g}\mathbf{Q_1} \\ &\quad\cdot[\mathbf{F}\boldsymbol{x}_2 + \mathbf{B}\boldsymbol{U} + \boldsymbol{d}(t) - \ddot{\boldsymbol{r}}]\Big\} \\ &= \boldsymbol{s}^T\{\dot{\boldsymbol{e}} + \frac{\gamma mh}{ng}\mathbf{Q_3}\dot{\boldsymbol{e}} + \frac{\alpha h}{g}\mathbf{Q_2}\dot{\boldsymbol{e}} + \frac{h}{\beta g}\mathbf{Q_1} \\ &\quad\cdot[\mathbf{F}\boldsymbol{x}_2 - \mathbf{F}\boldsymbol{x}_2 + \ddot{\boldsymbol{r}} - \frac{\beta g}{h}\dot{\boldsymbol{e}}^{2-h/g} - \frac{\beta\gamma m}{n}\mathbf{Q_3}\dot{\boldsymbol{e}}^{2-h/g} \\ &\quad - \alpha\beta\mathbf{Q_2}\dot{\boldsymbol{e}}^{2-h/g} - \boldsymbol{\varepsilon}\mathrm{sgn}(\boldsymbol{s}) + \boldsymbol{d}(t) - \ddot{\boldsymbol{r}}]\} \\ &= -\boldsymbol{s}^T\frac{h}{\beta g}\mathbf{Q_1}[\boldsymbol{\varepsilon}\mathrm{sgn}(\boldsymbol{s}) - \boldsymbol{d}(t)] \\ &= -|s_i|\frac{h}{\beta g}\dot{e}_i^{h/g-1}[\varepsilon_i - d_i(t)] \quad i = 1, 2, 3.\end{aligned}$$

Since g and h are positive odds and satisfy $1 < h/g < 2$, $\dot{e}_i^{h/g-1} > 0$ is always true when $\dot{e}_i \neq 0$. If $\varepsilon_i > |d_i(t)|$, then $\dot{V} = \boldsymbol{s}^T\dot{\boldsymbol{s}} \leq -\eta\|\boldsymbol{s}\|$ holds.

When $\dot{e}_i = 0$, substitute the control law (15) into (9) to obtain the following expression:

$$\ddot{\boldsymbol{e}} = \boldsymbol{d}(t) - \boldsymbol{\varepsilon}\mathrm{sgn}(\boldsymbol{s}).$$

Similarly, if $\varepsilon_i > |d_i(t)|$, then

$$\ddot{e}_i = d_i(t) - \varepsilon_i\mathrm{sgn}(s_i) \Rightarrow \begin{cases} \ddot{e}_i \leq -\eta \ s_i > 0 \\ \ddot{e}_i \geq \eta \ s_i < 0 \end{cases}.$$

According to Feng et al. [20], the system states that any initial position can converge to a sliding surface.

Negative power terms will not exist in the control law if $2 > h > g > 1$ and $m > n$. Therefore, the singularity problem in the conventional TSM method is completely solved.

As previously discussed, the derivative $\dot{V} = \boldsymbol{s}^T\dot{\boldsymbol{s}} \leq -\eta\|\boldsymbol{s}\|$ can be proved to always hold if the conditions $2 > h > g > 1$, $\varepsilon_i > |d_i(t)|(i = 1, 2, 3)$ and $m > n$ are satisfied. That is, for the nonlinear system described by (9) with the IFNTSM control law (15), the system states can converge to $\boldsymbol{s} = 0$. After the state variables reach the sliding surface, any initial error will eventually reach the state $\boldsymbol{e} = 0$, and the convergence time determined by T_{IFNi} is finite.

3.2 Novel Comprehensive IFNTSM–ESO Method

Aimed at the complex uncertainties in aircraft aerodynamic, center of gravity and inertial parameters, an ESO is designed to provide an effective method of estimating $\boldsymbol{d}(t)$ and then overcoming the drawback of large switching gains in sliding mode control caused by the strong uncertainties.

Define $\boldsymbol{D}(t) = \mathbf{F}\boldsymbol{x}_2 + \boldsymbol{d}(t)$ and expand it to the new system state variable x_3. The system (9) is expressed as follows:

$$\begin{cases} \dot{\boldsymbol{x}}_1 = \boldsymbol{x}_2 \\ \dot{\boldsymbol{x}}_2 = \mathbf{B}\boldsymbol{U} + \boldsymbol{x}_3 \\ \dot{\boldsymbol{x}}_3 = \boldsymbol{\xi} \end{cases}. \tag{16}$$

Subsequently, an observer is designed in (17) to simultaneously estimate the state $\boldsymbol{x}_1, \boldsymbol{x}_2$ and uncertain item $\boldsymbol{D}(t)$.

$$\begin{cases} \tilde{\boldsymbol{x}}_1 = \boldsymbol{z}_1 - \boldsymbol{x}_1 \\ \dot{\boldsymbol{z}}_1 = \boldsymbol{z}_2 - \beta_1 \tilde{\boldsymbol{x}}_1 \\ \dot{\boldsymbol{z}}_2 = \mathbf{B}\boldsymbol{U} + \boldsymbol{z}_3 - \beta_2 \boldsymbol{fal}_2(\tilde{\boldsymbol{x}}_1, \alpha_2, \delta_2) \\ \dot{\boldsymbol{z}}_3 = -\beta_3 \boldsymbol{fal}_3(\tilde{\boldsymbol{x}}_1, \alpha_3, \delta_3) \end{cases}, \tag{17}$$

where $\boldsymbol{z}_1, \boldsymbol{z}_2$, and $\boldsymbol{z}_3$ are estimations of the system states $\boldsymbol{x}_1, \boldsymbol{x}_2$, and uncertain item $\boldsymbol{D}(t)$, respectively, and $\tilde{\boldsymbol{x}}_1 = [\tilde{x}_{11}, \tilde{x}_{12}, \tilde{x}_{13}]^T$ represents the estimation error of $\boldsymbol{x}_1$; $\beta_i (i = 1, 2, 3)$ is the positive observer gain; and $\boldsymbol{fal}(\cdot)$ is the nonlinear function, which is defined as:

$$\begin{aligned} &\boldsymbol{fal}_j(\cdot) \\ &\quad = [fal_{j1}(\tilde{x}_{11}, \alpha_j, \delta_j), fal_{j2}(\tilde{x}_{12}, \alpha_j, \delta_j), fal_{j3}(\tilde{x}_{13}, \alpha_j, \delta_j)]^T \end{aligned}$$

$$fal_{ji}(\tilde{x}_{1i}, \alpha_j, \delta_j) = \begin{cases} \frac{\tilde{x}_{1i}}{\delta^{1-\alpha_j}} & |\tilde{x}_{1i}| \le \delta_j \\ |\tilde{x}_{1i}|^{\alpha_j} sign(\tilde{x}_{1i}), & |\tilde{x}_{1i}| > \delta_j \end{cases} \quad i = 1, 2, 3, \quad j = 2, 3,$$

where $0 < \alpha_j < 1$ and $\delta_j > 0$ are the observer coefficients to be designed.

Choose appropriate values of the observer gains β_i, α_j, δ_j. The observer states $\boldsymbol{z}_1$ and $\boldsymbol{z}_2$ tend to the original states $\boldsymbol{x}_1(t), \boldsymbol{x}_2(t)$, and the observer state $\boldsymbol{z}_3 = [z_{31}, z_{32}, z_{33}]^T$ tends to the system uncertainties $\boldsymbol{D}(t) = [D_1(t), D_2(t), D_3(t)]^T$.

Define the observer errors as

$$\begin{cases} \tilde{\boldsymbol{x}}_2 = \boldsymbol{z}_2 - \boldsymbol{x}_2 \\ \tilde{\boldsymbol{x}}_3 = \boldsymbol{z}_3 - \boldsymbol{x}_3 \end{cases},$$

where $\tilde{\boldsymbol{x}}_2 = [\tilde{x}_{21}, \tilde{x}_{22}, \tilde{x}_{23}]^T$ and $\tilde{\boldsymbol{x}}_3 = [\tilde{x}_{31}, \tilde{x}_{32}, \tilde{x}_{33}]^T$ denote the estimation error of $\boldsymbol{x}_2$ and $\boldsymbol{x}_3$.

Substituting (16) into (17) causes an error system

$$\begin{cases} \dot{\tilde{\boldsymbol{x}}}_1 = \tilde{\boldsymbol{x}}_2 - \beta_1 \tilde{\boldsymbol{x}}_1 \\ \dot{\tilde{\boldsymbol{x}}}_2 = \tilde{\boldsymbol{x}}_3 - \beta_2 \boldsymbol{fal}_2(\tilde{\boldsymbol{x}}_1, \alpha_2, \delta_2) \\ \dot{\tilde{\boldsymbol{x}}}_3 = \boldsymbol{\xi} - \beta_3 \boldsymbol{fal}_3(\tilde{\boldsymbol{x}}_1, \alpha_3, \delta_3) \end{cases}. \tag{18}$$

For the i-th element $\tilde{x}_{1i}$, we define the following functions:

$$g_1(\tilde{x}_{1i}) = \frac{1}{k_1} \frac{\beta_3 |fal_{3i}(\tilde{x}_{1i})|}{\beta_2 fal'_{2i}(\tilde{x}_{1i})},$$

$$h_2(\tilde{x}_{1i}, \tilde{x}_{2i}) = \tilde{x}_{2i} - \beta_1 \tilde{x}_{1i} + k_1 g_1(\tilde{x}_{1i}) sign(\tilde{x}_{1i}),$$

$$g_2(\tilde{x}_{1i}, \tilde{x}_{2i}) = \begin{cases} k_3 |h_2|, & |h_2| > g_1 \\ k_3 |g_1|, & |h_2| \le g_1 \end{cases},$$

$$\begin{aligned} h_3(\tilde{x}_{1i}, \tilde{x}_{2i}, \tilde{x}_{3i}) &= \tilde{x}_{3i} - \beta_2 fal_{2i}(\tilde{x}_{1i}) - \beta_1(\tilde{x}_{2i} - \beta_1 \tilde{x}_{1i}) \\ &\quad + k_2 g_2(\tilde{x}_{1i}, \tilde{x}_{2i}) sat(h_2/g_1), \end{aligned}$$

$$g_3(\tilde{x}_{1i}, \tilde{x}_{2i}, \tilde{x}_{3i}) = \begin{cases} |h_3|, & |h_3| > g_2 \\ g_2, & |h_3| \le g_2 \end{cases},$$

where $k_1 > 1$, $k_2 > 1$, and $k_3 > \frac{k_1(k_1+1)}{(k_2-1)} \left| \frac{dg_1}{d\tilde{x}_{1i}} \right|$.

Lemma 1 [31]. *For system (9) and the nonlinear extended state observer designed as (17), if the system disturbances satisfy $|\xi_i| < W$ and the observer parameters are properly chosen as (19), the trajectories of observer error system (18) will reach and be constrained in the area that contains the origin $G_0 = \left\{ (\tilde{x}_{1i}, \tilde{x}_{2i}, \tilde{x}_{3i}) : \beta_1 g_3 \le \frac{c}{c-1} W \right\}$ in a finite time, i.e., the observer errors converge to a small neighborhood around zero.*

$$\begin{aligned} \frac{\beta_1}{c} > (1 + 2k_2)k_3 + \left| \frac{\beta_2 fal'_{2i}}{k_3} - \beta_1 k_2 - k_2 \frac{\beta_3}{\beta_2} \left(\frac{fal_{3i}}{fal'_{2i}} \right)' + k_2^2 k_3 \right| \\ + \left| \frac{\beta_3}{\beta_2} \left(\frac{fal_{3i}}{fal'_{2i}} \right)' \right| + k_1(1 + k_2) \left| \frac{\beta_3}{\beta_2} \left(\frac{fal_{3i}}{fal'_{2i}} \right)' \right| \end{aligned}, \tag{19}$$

where $c > 1$.

Theorem 2 *Considering the nonlinear system (9)with the comprehensive IFNTSM–ESO control law obtained as (20), the system tracking error $\boldsymbol{e}$ can converge to zero in a finite time if conditions $2 > h > g > 1$, $\varepsilon_i > |D_i(t) - z_{3i}(t)|$ $(i = 1,2,3)$ and $m > n$ are satisfied, where z_{3i} is obtained from the nonlinear ESO (17) that satisfies Lemma 1.*

$$\begin{aligned} \boldsymbol{U} = -\mathbf{B}^{-1} \Bigg[&- \ddot{\boldsymbol{r}} + \frac{\beta g}{h} \dot{\boldsymbol{e}}^{2-h/g} + \frac{\beta \gamma m}{n} \mathbf{Q}_3 \dot{\boldsymbol{e}}^{2-h/g} \\ &+ \alpha\beta \mathbf{Q}_2 \dot{\boldsymbol{e}}^{2-h/g} + \boldsymbol{z}_3 + \boldsymbol{\varepsilon} \mathrm{sgn}(\boldsymbol{s}) \Bigg]. \end{aligned} \tag{20}$$

Proof Construct the Lyapunov function as follows:

$$V = \frac{1}{2} \boldsymbol{s}^T \boldsymbol{s}.$$

Differentiating it with respect to time along system (12) and (20) generates the following expression:

$$\begin{aligned} \dot{V} &= \boldsymbol{s}^T \Bigg\{ \dot{\boldsymbol{e}} + \frac{\gamma m h}{n g} \mathbf{Q}_3 \dot{\boldsymbol{e}} + \frac{\alpha h}{g} \mathbf{Q}_2 \dot{\boldsymbol{e}} + \frac{h}{\beta g} \mathbf{Q}_1 \\ &\quad \cdot [\mathbf{F}\boldsymbol{x}_2 + \mathbf{B}\boldsymbol{U} + \boldsymbol{d}(t) - \ddot{\boldsymbol{r}}] \Bigg\} \\ &= \boldsymbol{s}^T \Bigg\{ \dot{\boldsymbol{e}} + \frac{\gamma m h}{n g} \mathbf{Q}_3 \dot{\boldsymbol{e}} + \frac{\alpha h}{g} \mathbf{Q}_2 \dot{\boldsymbol{e}} + \frac{h}{\beta g} \mathbf{Q}_1 \\ &\quad \cdot \Bigg[-\frac{\beta g}{h} \dot{\boldsymbol{e}}^{2-h/g} - \frac{\beta \gamma m}{n} \mathbf{Q}_3 \dot{\boldsymbol{e}}^{2-h/g} \\ &\quad - \alpha\beta \mathbf{Q}_2 \dot{\boldsymbol{e}}^{2-h/g} - \boldsymbol{\varepsilon}\, \mathrm{sgn}(\boldsymbol{s}) + \boldsymbol{D}(t) - \boldsymbol{z}_3(t) \Bigg] \Bigg\} \end{aligned}$$

$$= -\boldsymbol{s}^T \frac{h}{\beta g} \mathbf{Q_1}[\boldsymbol{\varepsilon}\,\mathrm{sgn}(\boldsymbol{s}) - (\boldsymbol{D}(t) - \boldsymbol{z}_3(t))]$$
$$= -|s_i| \frac{h}{\beta g} \dot{e}_i^{h/g-1}[\varepsilon_i - (\boldsymbol{D}_i(t) - z_{3i}(t))] \quad i = 1, 2, 3.$$

Based on Lemma 1, the observer errors converge to a small neighborhood around zero G_0, which indicates that the observer can obtain an estimate of uncertainties $D_i(t)$ with a bounded error. According to Theorem 1, the inequality $\dot{V} \leq -\eta\|\boldsymbol{s}\|$ and the reachability of the sliding surface are satisfied and always holds when $\varepsilon_i > |D_i(t) - z_{3i}(t)|$. Consequently, the system tracking error will reach $\boldsymbol{e} = 0$ in a finite time due to the characteristics of the sliding manifold (12).

According to Theorem 2, the system stability conditions change to $\varepsilon_i > |D_i(t) - z_{3i}(t)|$ $(i = 1, 2, 3)$ for the novel control law (20). Compared with the original $\varepsilon_i > |d_i(t)|$, we can easily observe that the switching gains $\boldsymbol{\varepsilon} = [\varepsilon_1, \varepsilon_2, \varepsilon_3]^T$ in the control laws may decrease from the upper bound of the unknown uncertainties $|d_i(t)|$ to the observer errors $|D_i(t) - z_{3i}(t)|$ due to introduction of the ESO. The gains of noncontinuous items in the novel IFNTSM–ESO method decrease in most cases and the chattering phenomenon can be effectively alleviated. The maximum limits of uncertainties that the control system can handle are broken and the ability of the system to address large disturbances and uncertainties is improved.

4 Simulation Results

Numerical simulation results are provided to demonstrate the ability of IFNTSM–ESO to improve the convergence rate and effectively address parameter uncertainties.

A certain blended wing body (BWB) aircraft model is considered as the nonlinear controlled object. The aircraft model is a typical BWB aircraft that uses the high-aspect ratio tailless configuration, as shown in Fig. 1. A multi-control surface scheme is realized in this aircraft to provide control for the roll, pitch, and yaw channels. Two sets of elevons on the trailing edge of left and right wings, i.e., inner and outer elevons, are used to control the pitch and roll motion of the BWB aircraft by the coordinate deflections and differential deflections of the elevons, respectively. A set of split drag rudders on the wingtips is used to control the yaw motion.

The basic parameters of the BWB aircraft are listed in Table 1, and the saturation and rate limits of the control actuators are denoted in Table 2.

The initial condition of the BWB aircraft is set to the altitude $h_0 = 12$ km, the Mach number Ma $= 0.6$, $\phi_0 = 0°$, $\psi = 0°$, $\theta = 3.85°$, and the angular velocity $p = q = r = 0$ rad/s. The range of uncertainties in the CG, aerodynamic and inertial parameters is set to $[10\%c_A, 2\%c_A, 2\%c_A]$, $\pm 30\%$, and $\pm 30\%$.

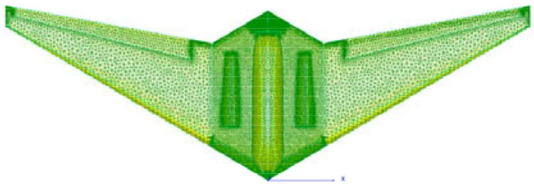

Fig. 1 Layout of the blended wing body aircraft

Table 1 BWB aircraft parameters

Parameters	Value
Weight, kg	109,260
Wing area, m^2	407
Wing span, m	72.9
Mean aerodynamic chord, m	7.8
Moment of inertia I_x, kgm^2	2,007,535
Moment of inertia I_y, kgm^2	2,183,303
Moment of inertia I_z, kgm^2	1,128,960
Product of inertia I_{xz}, kgm^2	− 71,383
Flight height, km	12
Ma	0.6
Trim angle of attack, deg	3.85
Zero angle-of-attack lift coefficient	0.1752
Derivative of lift coefficient	5.36
Lift-to-drag ratio	31.8

Table 2 Saturation and rate limits of the actuators

	Inner elevon	Outer elevon	Split drag rudder
Deflection limit, deg	[− 20,20]	[− 20,20]	[− 20,20]
Rate limit, deg/s	[− 100,100]	[− 100,100]	[− 100,100]

The sgn(·) function that is involved in (15) and (20) produces chattering phenomena in the system. To further solve the problem of oscillation, a continuous function is proposed instead as follows:

$$\dot{s}_i = \varepsilon_i \cdot \frac{s_i}{|s_i| + \sigma}.$$

To prove the performance of the IFNTSM method in the convergence rate, we compare the conventional and proposed methods by flight simulation. NTSM and FNTSM are employed for contrast as the conventional methods. Square wave command signals of 5° and 4° are given to the roll and pitch channels of the aircraft. Each command begins at 2 s and ends at 8 s. Figures 2, 3 and 4 show a comparison of the attitude response among the three different control

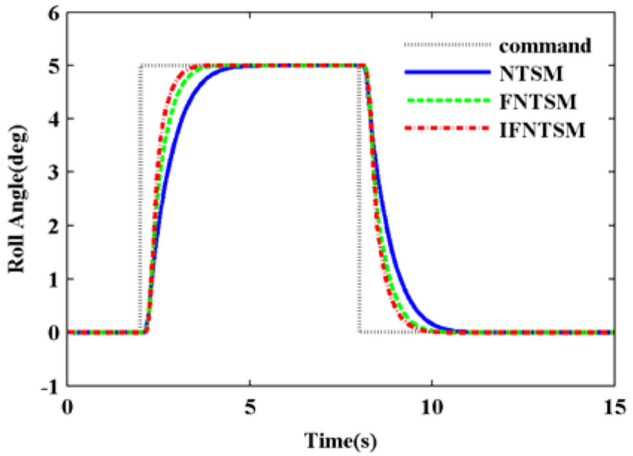

Fig. 2 Roll angle responses

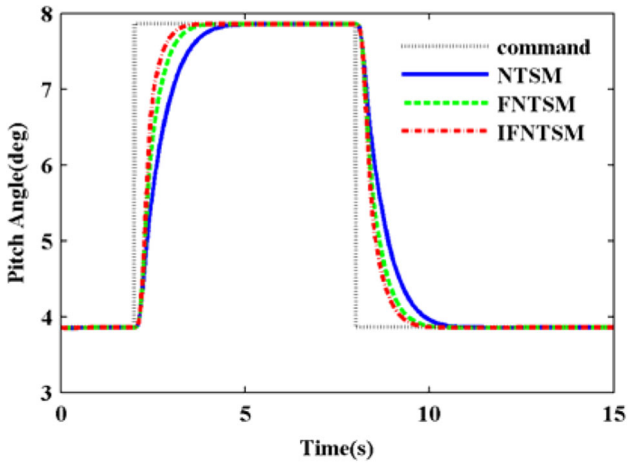

Fig. 3 Pitch angle responses

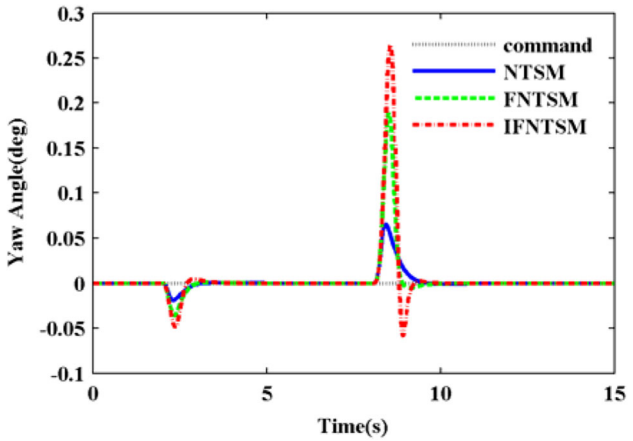

Fig. 4 Yaw angle responses

laws. The corresponding parameters of the three controllers are listed in Table 3.

As shown in Figs. 2, 3 and 4, compared with the conventional methods of SMC, the IFNTSM method definitely improves the response performance of aircraft. The detailed numerical comparison results of the three controllers are listed in Table 4.

Table 3 Control parameters of the three different methods

	Sliding surface							Reaching law	
	α_i	β_i	γ_i	h	g	m	n	ε_i	δ_i
NTSM	1	–	–	13	11	–	–	20	0.8
FNTSM	1	1	–	13	11	11	9	20	0.8
IFNTSM	1	1	1	13	11	11	9	20	0.8

Table 4 Comparison of tracking speed of different controllers

	Attitude command (deg)	Steady-state errors (deg)	Settling time (s)		
			NTSM	FNTSM	IFNTSM
Pitch channel	4	0.0020	3.049	2.116	1.828
Roll channel	5	0.0025	3.267	2.270	1.696

As shown in Table 4, the response speeds of the IFNTSM in the pitch channel and roll channel increase by 40.0% and 48.1%, respectively, compared with the NTSM, and increase by 13.6% and 25.3%, respectively, compared with the FNTSM.

We introduce parameter uncertainties into the aircraft model, and the similar square wave commands are given to the model, which verifies the robustness performance of the IFNTSM–ESO method. The parameter uncertainties are denoted as follows:

a. CG uncertainty:

$$\left[\Delta x_{cg}\ \Delta y_{cg}\ \Delta z_{cg}\right] = \left[10\%c_A\ 2\%c_A\ 2\%c_A\right].$$

b. Aerodynamic parameter uncertainty:

$$k_C = -30\% \sim 30\%.$$

c. Inertial parameter uncertainty:

$$k_I = -30\% \sim 30\%.$$

These parameter uncertainties are usually assumed to be known and time varying. In the simulation, we define the uncertainties as their boundary value and introduce parameter uncertainties in the fifth second.

Assume that these uncertainties are continuous in the aircraft model. Figures 5, 6 and 7 show the attitude tracking performance of the IFNTSM controller in all channels of aircraft attitude. Figures 8, 9 and 10 depict the attitude tracking performance of the comprehensive IFNTSM–ESO controller

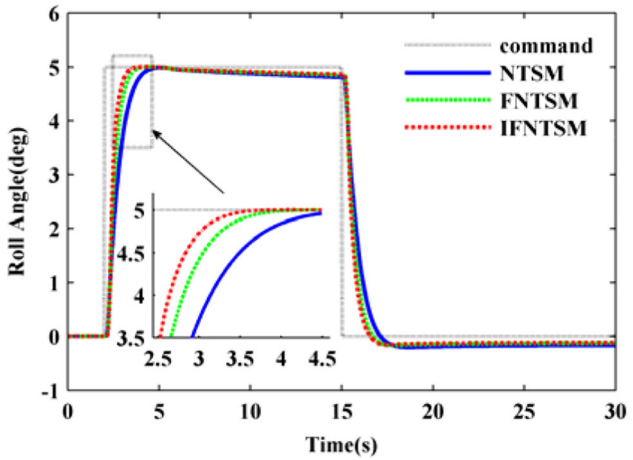

Fig. 5 IFNTSM roll response with uncertainties

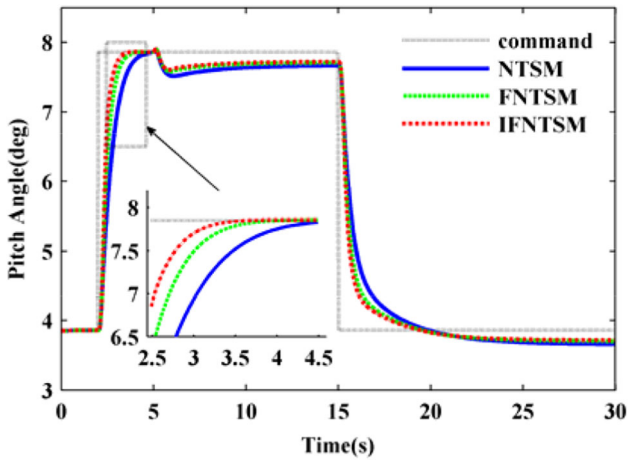

Fig. 6 IFNTSM pitch response with uncertainties

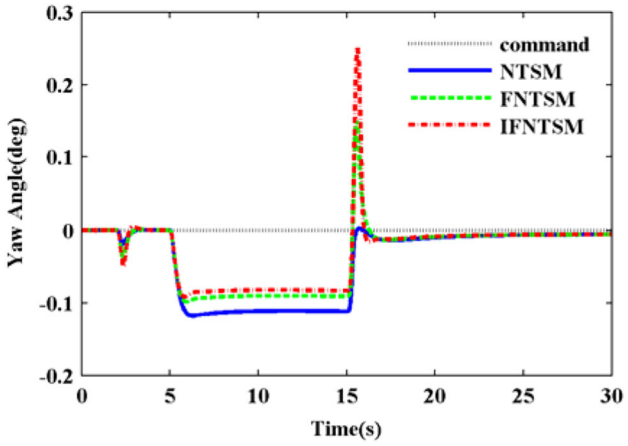

Fig. 7 IFNTSM yaw response with uncertainties

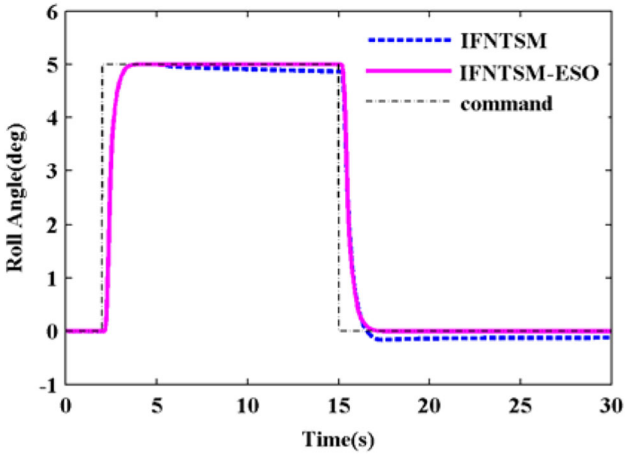

Fig. 8 IFNTSM–ESO roll response with uncertainties

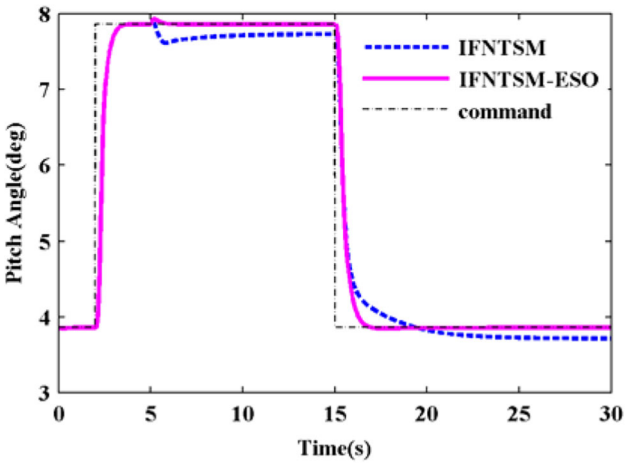

Fig. 9 IFNTSM–ESO pitch response with uncertainties

in the three channels to verify the ability of the ESO to address strong system uncertainties. Figures 11 and 12 show the comparison of the attitude response between IFNTSM–ESO and NTSM–ESO. The corresponding actuator deflections are shown in Fig. 13.

As shown in Figs. 5, 6 and 7, the uncertainties lead to large deviations in the attitude angles, especially in the pitch axis, and that is because the CG uncertainty Δx_{cg} is much larger than Δy_{cg} and Δz_{cg}.

And the partial enlarged drawings in Figs. 5 and 6 illustrate that the IFNTSM method definitely improves the response performance of aircraft. However, the parameter uncertainties have a negative effect on the IFNTSM control performance. The attitude responses in all attitude channels can also track the commands in the presence of certain errors.

When the nonlinear observer is introduced to estimate and compensate the system uncertainties, the tracking performance of the controller is significantly improved in all channels, which indicates that the ability of the control system to address uncertainties is enhanced and the robust performance of the system is considerably increased. This simulation test effectively proves the robustness and capa-

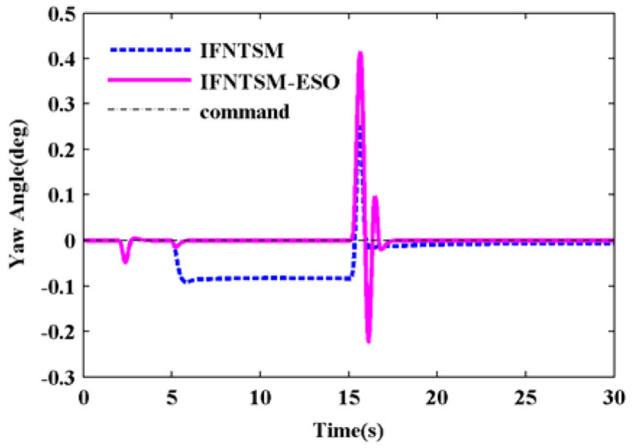

Fig. 10 IFNTSM–ESO yaw response with uncertainties

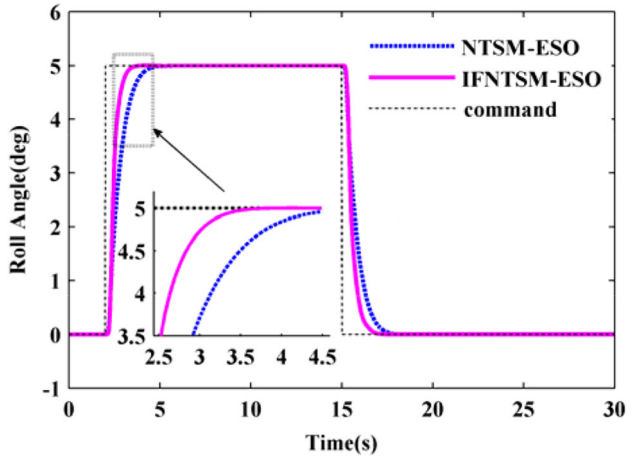

Fig. 11 Comparison of the roll response between IFNTSM–ESO and NTSM–ESO

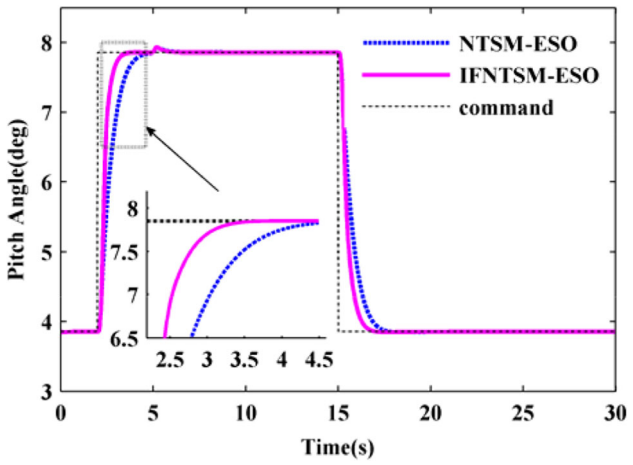

Fig. 12 Comparison of the pitch response between IFNTSM–ESO and NTSM–ESO

bility in handling the problem of parameter uncertainties of the IFNTSM–ESO method.

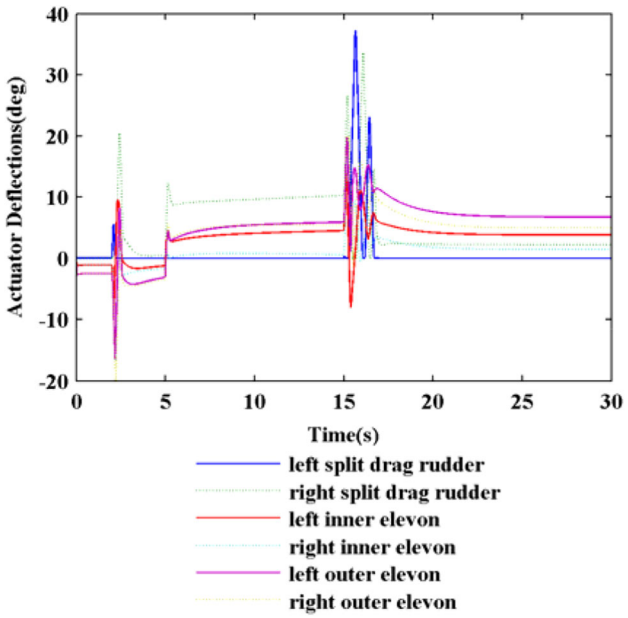

Fig. 13 IFNTSM–ESO actuator deflections

Table 5 Comparisons of the peak value in the yaw channel

	NTSM	FNTSM	IFNTSM
Peak value, deg (with uncertainty)	0.027	0.1498	0.2502
Peak value, deg (without uncertainty)	0.0487	0.1685	0.2859

As shown in Figs. 11 and 12, both the IFNTSM–ESO method and NTSM–ESO method show excellent robustness against parameter uncertainties due to the introduction of the nonlinear observer. The proposed IFNTSM–ESO method is superior in the finite-time convergence speed to NTSM–ESO due to the novel nonlinear sliding mode surface.

As shown in Figs. 4, 7 and 10, the IFNTSM method seems to increase the peak value in the yaw channel. The comparisons of the peak value of the different three control laws, i.e., NTSM, FNTSM, IFNTSM, are listed in Table 5. This is mainly because the larger control deflections of the IFNTSM produces a stronger lateral and directional coupling effect.

In addition, the influence of different values of the control parameter ε on the response performance of IFNTSM–ESO is shown in Figs. 14 and 15. The uncertainty in each channel and its estimation value from the ESO are shown in Figs. 16, 17 and 18.

As shown in Figs. 14 and 15, the roll and pitch responses show relatively similar performance for three typical values $\varepsilon = 6$, 10, and 20, which indicates that different values of the control parameters ε have a minimal effect on the control performance of IFNTSM–ESO.

As shown in Figs. 16, 17 and 18, the ESO designed in this paper can precisely estimate the uncertainty of aerodynamic, center of gravity and inertia parameters in each channel. The

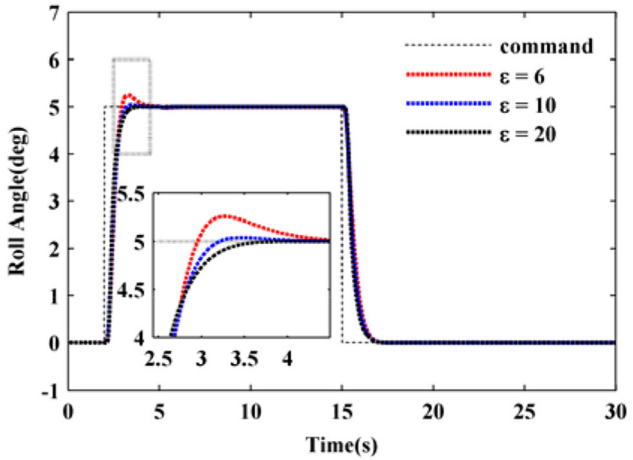

Fig. 14 IFNTSM–ESO roll response with different ε

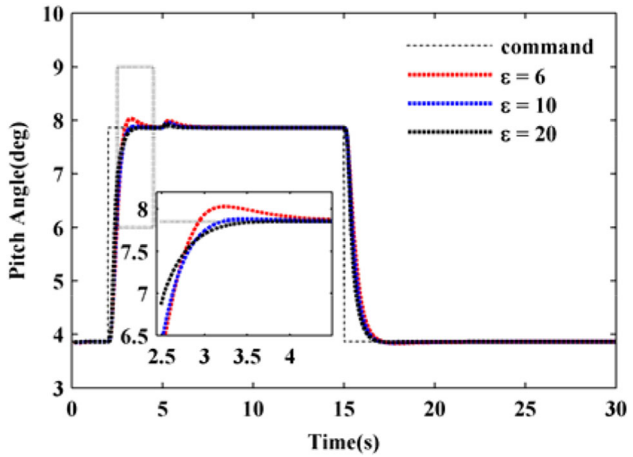

Fig. 15 IFNTSM–ESO pitch response with different ε

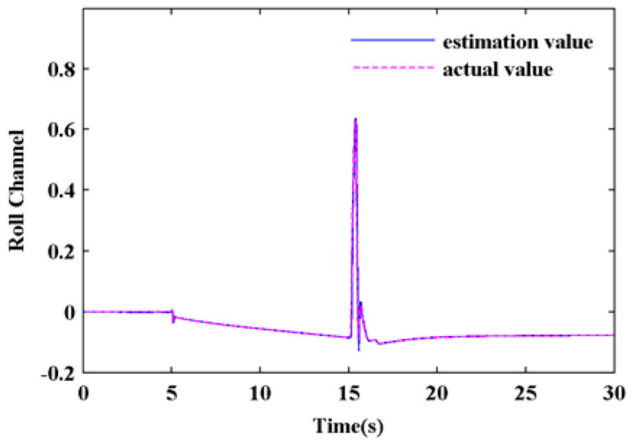

Fig. 16 Estimation value of D(t) in the roll channel

combination of the ESO and sliding mode controller achieves excellent tracking performance and shows superior ability while handling parameter uncertainties.

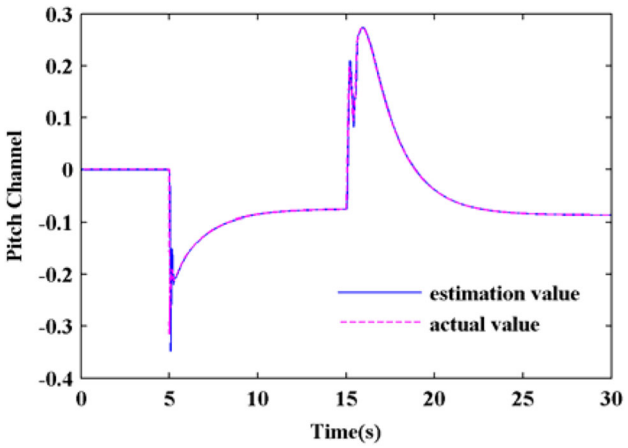

Fig. 17 Estimation value of D(t) in the pitch channel

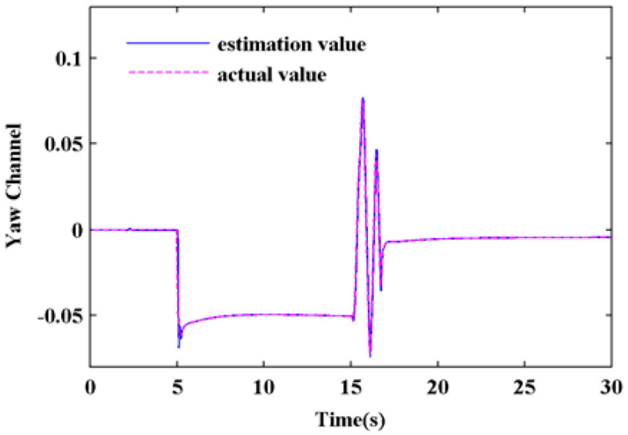

Fig. 18 Estimation value of D(t) in the yaw channel

The simulation results demonstrate the effectiveness of the proposed IFNTSM–ESO method in quick convergence and outstanding robust performance properties.

5 Conclusion

In this paper, a comprehensive IFNTSM–ESO controller design is developed for aircraft subject to composite uncertainties in aerodynamic, center of gravity and inertial parameters. A 6-DoF aircraft model with parameter uncertainties is established. Then, the robust IFNTSM–ESO control method is proposed, which combines the advantages of IFNTSM control and ESO. For any initial state, IFNTSM can guarantee a fast rate for convergence and finite time to attain equilibrium. The introduction of the ESO can overcome the drawback of large switching gains in the sliding mode controller and effectively improve robustness to system parameter variations. Aircraft flight simulations are performed to prove the capability of the IFNTSM–ESO controller in addressing the problem of parameter uncertainties and accelerating the con-

vergence rate. The results of the simulations verify that the proposed method can precisely and rapidly track the command signals in all three channels of aircraft in the presence of complex parameter uncertainties.

Acknowledgments This study has been supported by the National Natural Science Foundation of China (Grant No. 61273099, 61304030).

References

1. Khammash M, Zou L, Almquist JA et al (1999) Robust aircraft pitch-axis control under weight and center of gravity uncertainty. In: Proceedings of the IEEE conference on decision and control, Phoenix, AZ, USA, vol 2, pp 1970–1975. https://doi.org/10.1109/cdc.1999.830925
2. Hentabli K, Akhrif O, Saydy L (2003) Robust longitudinal flight control system under weight and center of gravity uncertainty. In: Proceedings international conference on electrical, electronic and computer engineering, Montreal, Quebec, Canada, pp 1743–1748. https://doi.org/10.1109/ccece.2003.1226247
3. Islam S, Liu PX, Saddik AE (2015) Robust control of four-rotor unmanned aerial vehicle with disturbance uncertainty. IEEE Trans Ind Electron 62(3):1563–1571. https://doi.org/10.1109/tie.2014.2365441
4. Wenyan B, Sen C, Kunfeng L et al (2017) Stable and robust control design for a benchmark hypersonic aircraft model. Proc CCC Dalian 2017:3443–3448. https://doi.org/10.23919/ChiCC.2017.8027891
5. Cacan MR, Costello M (2018) Adaptive control of precision guided airdrop systems with highly uncertain dynamics. J Guid Control Dyn 41(5):1–11. https://doi.org/10.2514/1.g003039
6. Tol HJ, DeVisser CC, Sun LG et al (2016) Multivariate spline-based adaptive control of high-performance aircraft with aerodynamic uncertainties. J Guid Control Dyn 39(4):1–20. https://doi.org/10.2514/1.g001079
7. Somanath A, Annaswamy A (2010) Adaptive control of hypersonic vehicles in presence of aerodynamic and center of gravity uncertainties. In: Proceedings of the IEEE conference on decision and control, Atlanta, GA, USA, pp 4661–4666. https://doi.org/10.1109/cdc.2010.5717494
8. Kamalapurkar R, Bialy B, Andrews L et al (2013) Adaptive RISE feedback control strategies for systems with structured and unstructured uncertainties. In: Proceedings of AIAA guidance, navigation, and control conference, Boston, MA, USA, pp 1–11. https://doi.org/10.2514/6.2013-4852
9. VanGils P, VanKampen E, DeVisser CC et al (2016) Adaptive incremental backstepping flight control for a high-performance aircraft with uncertainties. In: Proceedings of the AIAA guidance, navigation, and control conference, San Diego, CA, USA, 2016, pp 1–26. https://doi.org/10.2514/6.2016-1380
10. Maity A, Höcht L, Heise C et al (2018) Adaptive optimal control using frequency selective information of the system uncertainty with application to unmanned aircraft. IEEE Trans Cybern 48(1):165–177. https://doi.org/10.1109/TCYB.2016.2627030
11. Diepolder J, Göttlicher C, Grüter B et al (2017) Optimal control based flight control law testing with parameter uncertainties. In: Proceedings o IEEE conference control technol. Appl. (CCTA), Mauna Lani, HI, USA, pp 1432–1437. https://doi.org/10.1109/ccta.2017.8062660
12. Gottlicher C, Gnoth M, Bittner M et al (2016) Aircraft parameter estimation using optimal control methods. In: Proceedings of AIAA atmospheric flight mechanics conference, San Diego, CA, USA, pp 1–18. https://doi.org/10.2514/6.2016-1534
13. Bluman JE, Kang CD, Shtessel Y (2018) Control of a flapping-wing micro air vehicle: sliding-mode approach. J Guid Control Dyn 41(5):1219–1225. https://doi.org/10.2514/1.g003160
14. Boukadida W, Benamor A, Messaoud H (2017) Optimal sliding mode control for a class of uncertain discrete-time systems. In: Proceedings of 16th international conference on sciences and techniques of automatic control and computer engineering (STA), Monastir, Italy, pp 635–340. https://doi.org/10.1109/sta.2017.8314886
15. Abdulhamitbilal E, Jafarov EM (2012) Robust sliding mode speed hold control system design for full nonlinear aircraft model with parameter uncertainties: A step beyond. In: Proceedings of the 12th international workshop on variable structure systems, Mumbai, Maharashtra, India, 2012, pp 7–15. https://doi.org/10.1109/vss.2012.6163470
16. Abdulhamitbilal E (2014) Robust flight sliding modes control system design for nonlinear aircraft with parameter uncertainties. In: Proceedings of the 13th international workshop on variable structure systems (VSS), Nantes, France, 2014, pp 1–6. https://doi.org/10.1109/vss.2014.6881127
17. Xiong JJ, Zhang G (2016) Sliding mode control for a quadrotor UAV with parameter uncertainties. In: Proceedings of the international conference on control, Hong Kong, 2016, pp 207–212. https://doi.org/10.1016/j.isatra.2016.09.019
18. Man Z, Yu X (1996) Terminal sliding mode control of MIMO linear systems. In: Proceedings of the IEEE conference on decision and control, Kobe, Japan, 1996, pp 4619–4624. https://doi.org/10.1109/81.641769
19. Wu Y, Yu X, Man Z (1998) Terminal sliding mode control design for uncertain dynamic systems. Syst Control Lett 34(5):281–287. https://doi.org/10.1016/S0167-6911(98)00036-X
20. Feng Y, Yu X, Man Z (2002) Non-singular terminal sliding mode control of rigid manipulators. Automatica 38(12):2159–2167. https://doi.org/10.1016/S0167-6911(98)00036-X
21. Lin C (2006) Nonsingular terminal sliding mode control of robot manipulators using fuzzy wavelet networks. IEEE Trans Fuzzy Syst 14(6):849–859. https://doi.org/10.1109/tfuzz.2006.879982
22. Jin M, Lee J, Chang PH (2009) Practical nonsingular terminal sliding-mode control of robot manipulators for high-accuracy tracking control. IEEE Trans Ind Electron 56(9):3593–3601. https://doi.org/10.1109/tie.2009.2024097
23. Han J (2009) From PID to active disturbance rejection control. IEEE Trans Ind Electron 56(3):900–906. https://doi.org/10.1109/TIE.2008.2011621
24. Cui R, Chen L, Yang C et al (2017) Extended state observer-based integral sliding mode control for an underwater robot with unknown disturbances and uncertain nonlinearities. IEEE Trans Ind Electron 64(8):6785–6795. https://doi.org/10.1109/TIE.2018.2868034
25. He M, He J (2018) Extended state observer-based robust backstepping sliding mode control for a small-size helicopter. IEEE Access 6:33480–33488. https://doi.org/10.1109/ACCESS.2018.2845134
26. Shi S, Li J, Fang Y (2018) Extended-state-observer-based chattering free sliding mode control for nonlinear systems with mismatched disturbance. IEEE Access 6:22952–22957. https://doi.org/10.1109/ACCESS.2018.2828868
27. Zhao L, Li Q, Liu B et al (2017) Trajectory tracking control of a one degree of freedom manipulator based on a switched sliding mode controller with a novel extended state observer framework. IEEE Trans Syst Man Cybern Syst 25:64
28. Zhang J, Yang L, Shen G (2009) Modeling and attitude control of aircraft with center of gravity variations. Proc IEEE Aeros Conf 2009:1–11. https://doi.org/10.1109/AERO.2009.4839615
29. Yu X, Man Z (2002) Fast terminal sliding-mode control design for nonlinear dynamical systems. IEEE Trans Circuit Syst 49(2):261–264. https://doi.org/10.1109/81.983876

30. Yan J, Zhang J, Liu P et al (2017) A new IFNTSM controller design for the BWB aircraft with parameter uncertainties. Chinese Automation Congress (CAC). Jinan 2017:6167–6171. https://doi.org/10.1109/CAC.2017.8243888
31. Wan H (2001) Stability and application for active-disturbance-rejection-controller. Ph.D dissertation, Academy of Mathematics and Systems Science, Chinese Academy of Sciences, Beijing, China